Power Line Communications for Low-Voltage Power Grid Tomography

Mohamed O. Ahmed, *Student Member, IEEE*, and Lutz Lampe, *Senior Member, IEEE*

***Abstract*—Power line communications (PLC) has attracted considerable attention for supporting smart grid applications. Since it reuses the existing grid infrastructure, it offers cost advantages over alternative communications methods and gives electric utilities control over the communications medium. Furthermore, the "through-the-grid" property of PLC extends its possible use beyond mere communications. Since the PLC signals are bound to travel through the power grid, they can also be used for inference tasks, such as online diagnostics of power line integrity. In this paper, we consider such an inference application of PLC, enabled by modern signal processing. We assume a power grid at whose edges PLC devices are deployed to form a PLC network for purposes such as advanced meter reading. We are interested in retrieving the physical power-grid topology, i.e., the connections and lengths of power lines reaching to the locations of the PLC devices. To this end, we propose the combination of PLC-based ranging with inference based on end-to-end measurements. In the context of communication networks, the latter is known as tomography and hence, we refer to the developed method as power grid tomography. For the purpose of ranging we formulate a new super-resolution ranging algorithm specifically tailored for signal propagation through power lines. Numerical results for low-voltage distribution grid examples demonstrate the successful reconstruction of the grid topology by the proposed power grid tomography method.**

***Index Terms*—Power line communications, smart grid, diagnostics, inference, ranging, network tomography.**

I. Introduction

THE reuse of power lines for telephony and data communications, which is collectively referred to as power line communications (PLC), has a long history in supporting the operation of electric power companies, e.g. [1]–[5]. While early PLC has mainly employed narrowband communication formats, broadband PLC solutions have emerged in the late 1990ies [6], [7]. Moreover, the modern communication methods developed for high-speed PLC for Internet access and multimedia applications have recently migrated back to PLC systems considered by electric utilities for enabling the smart grid. This particularly applies to the use of orthogonal frequency-division multiplexing (OFDM) transmission, which has been adopted in broadband and narrowband PLC standards such as IEEE 1901[1], ITU-T G.9960, and ITU-T G.9902-04 and the forthcoming IEEE 1901.2 standard, respectively. The main advantage of PLC over other wired and wireless communication solutions is that its communications medium is in place and under the control of the electric utilities. This and the abilities of modern PLC technology have made it an attractive choice for communications for smart grids [5], [9], [10].

But PLC can be more than a means of communications in the context of smart grids. Since PLC is a "through the grid" [5] technology, it can provide status information about lines, loads, switches, etc. For example, joint sensing-and-communication devices use PLC to transfer data for online diagnostics, e.g. [5], [11]. Furthermore, features of the PLC signal itself can be used for grid monitoring. This includes fault localization, which can be done by measuring traveling waves from faults at different ends of power lines [12, Ch. 7] or by sending a stimulating signal which propagates along the line and reflects at the fault location. Examples of the latter are the time-domain reflectometry and impulse-response based methods using narrowband PLC signals to locate faults and impedance mismatches presented in [13] and [14], respectively. Another method, suggested in [15], considers the strength of the PLC signals received from smart meters as an indicator for predicting line failures.

In this paper, we consider the dual use of PLC for data communications and diagnostics. In particular, we apply the through-the-grid paradigm for inferring the physical topology of distribution power grids. The main premise is that PLC-enabled devices are in place at various loads (smart meters, energy storage modules, transformers, etc.) of a smart grid, and that their communications ability can be leveraged for grid monitoring tasks. Our work is related to reflectometry-based inference introduced in [16] and [17], which attempts to reconstruct the grid topology based on single-ended PLC signal measurements. However, this approach has strict limitations for the physical extension and/or complexity of the topology to be inferred. For example, [16] considers networks with very short cables and uses a signal bandwidth of about 500 MHz, which is not applicable for distribution power grids. The reflectometry approach in [17] targets the low-voltage (LV) distribution domain, but reconstruction of topologies with more than two or three branches is hardly possible due to strong attenuation of reflected signals traveling large distances. Another recent and related work is [18], [19], which investigates the use of PLC for distance measurement between

Manuscript received March 29, 2013; revised September 1, 2013. The editor coordinating the review of this paper and approving it for publication was S. Galli.

Part of this work has been presented at the IEEE International Conference on Smart Grid Communications, 2013. This work was supported by the National Sciences and Engineering Research Council of Canada (NSERC).

The authors are with the Department of Electrical and Computer Engineering, University of British Columbia, Vancouver, BC, Canada (e-mail: {mohameda, Lampe}@ece.ubc.ca).

Digital Object Identifier 10.1109/TCOMM.2013.111613.130238

[1]IEEE 1901 includes two different PHY layers, one referred to as windowed OFDM modulation and the other as Wavelet-OFDM [8].

distributed energy sources (DESs) in smart micro grids, so as to optimize the use of DESs with minimal energy losses. This has been extended to topology estimation in [20], which however assumes that, different from our work here, all branch points of the grid are equipped with PLC modems.

The new method we propose for topology inference in power distribution grids builds on two main ingredients, which are combined here for the first time: *PLC-based ranging* and *network tomography*. The former, similar to [18], uses PLC for the measurement of distances in the power grid. Different from [18], we do not apply a phenomenological but a deterministic, bottom-up PLC channel modeling approach, cf. e.g. [21], [22] and [3, Ch. 2]. This allows us (i) to capture the dependencies between transfer functions of different links in a PLC network and (ii) to devise a new parametric ranging method. Since the parametric method relies on the description of signal propagation through power lines by transmission line theory, its accuracy is not bounded by the bandwidth of the PLC signal used for ranging. Hence, it is a super-resolution technique [23, Ch. 4]. On the other hand, it requires that certain modeling assumptions hold true. Having collected ranging measurements from pairs of nodes in the grid, we use network tomography to infer the grid structure. Tomography is a methodology that tries to reconstruct the internal properties of an object based on observations from sensors surrounding it. It has been used in communication networks for inferring link performance, traffic matrices, and routing topologies based on end-to-end measurements, cf. e.g. [24]. By formulating power-grid-topology inference using distance measurements as a tree estimation problem, it becomes analogous to those considered in the communication network applications. Hence, we refer to the proposed method as PLC-based power grid tomography. Using typical LV grid structures and power cable examples, we present extensive numerical simulation results that demonstrate the performance of the proposed ranging method and the abilities of PLC-based *power grid tomography*

In this paper we provide a method for topology inference without elaborating on a specific application. However, we would like to point out three possible application areas. The first is the development and testing of PLC technology for smart grid, which, since the PLC network follows the physical topology of the power grid, requires accurate grid models. Since such information is generally not available and sometimes, in the LV domain, not even known to electric utility companies, our method is a valuable tool to obtain topology information through in-situ measurement. In fact, the lack of deterministic and statistical models for distribution grids needed to study PLC networking protocols for smart grids (e.g., [25], [26]) was our original motivation behind this work. The second use is to support PLC routing. Recently, the use of location information by way of geographic routing has been introduced to PLC in [27]. The proposed power grid tomography would provide the required location information, which is alike the role of grid location services in geographic routing for wireless communication networks [28]. A third application area, of perhaps the most immediate commercial potential and broader interest, is the support of the smart grid operation through online monitoring and diagnostics. This includes distance measurement and neighborhood inference as considered in [18], [19], and more generally online monitoring of grid elements including loads and lines, similar to the application examples considered in [13]–[15]. Furthermore, smart fault location systems using intelligent electronic devices (IEDs) as discussed in [29] would also benefit from updated grid-topology information. For example, power losses or PLC signal attenuation could be related to the line length obtained from power grid tomography to infer about the integrity of a power line.

The remainder of this paper is organized as follows. In Section II, we introduce the abstract model of the power grid used throughout the paper and define the objective of this work. We then describe PLC-based ranging, including the new parametric ranging algorithm, and network tomography applied to ranging measurements in Section III and IV, respectively. Together, these represent the new PLC-based power grid tomography method. Extensive numerical results are presented and discussed in Section V. Final remarks in Section VI conclude this paper.

II. System Model and Objective

We consider a part of the electricity grid in which a number of grid elements are PLC enabled. We refer to these elements as nodes, which emphasizes their participation in a PLC network and also the representation in a graphical grid model. We assume that these elements are connected through power lines forming a tree structure. This is often the case in the LV distribution domain of the grid, but it would also fit the wiring practices applied in many buildings. Examples for tree topologies considered in the literature include LV power distribution networks in residential areas for access [3, Figure 2.16], [30], [31] and smart meter reading [32] via PLC, random tree models for distribution networks [25], models for smart micro grids [18], and indoor power distribution installations [3, Figure 2.47], [30]. In the case of ring or mesh grids, tree topologies may still be realized for large periods of time, since loops are often open due to opened switches.

Figure 1(a) shows an example for a topology, in which power lines branching off a main supply line connect a number of loads, which could be, for example, houses in a residential area [31] or distributed energy sources and consumers in a micro grid [18]. PLC modems are deployed at the load locations, e.g., through the use of smart meters in the residential-area scenario. The PLC modems may be part of an existing PLC network that, with the PLC tomography proposed in this paper, can be used for topology inference and online grid monitoring, or may be put in place for the express purpose of doing these tasks. As also indicated in Figure 1(a), there may be open-ended branches or loads without PLC modems. Furthermore, branch points would not be easily accessible and thus not naturally be equipped with a PLC modem.

Figure 1(b) shows the sub-graph of the topology in Figure 1(a) at whose leaf nodes PLC modems are deployed. We observe that branches without PLC modems have been removed. The tree topology as shown in Figure 1(b) is what can be reconstructed by use of PLC technology, in particular the proposed PLC tomography method. The tree is described by a set of vertices or nodes $\mathcal{V}$, which includes leaf nodes

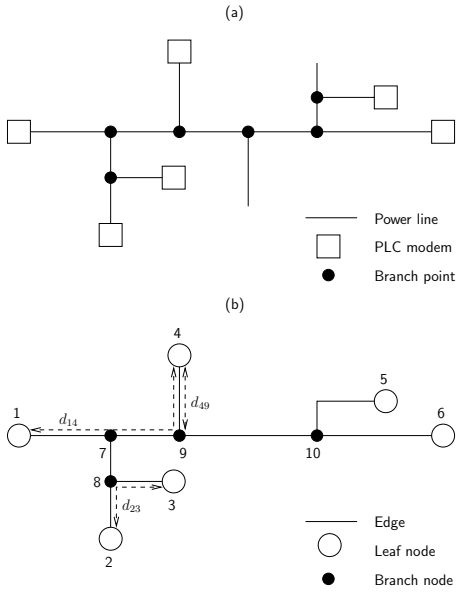

Fig. 1. (a) Example of a power line network topology. (b) Sub-graph with PLC modems at leaf nodes. Dashed-lines indicate node-to-node distances for three sample node pairs.

(outer vertices, grid elements equipped with PLC modems) and branch nodes (internal vertices, grid branch points), and a set of edges $\mathcal{E}$ (the power line segments). In Figure 1(b) we have enumerated the vertices and labeled a number of edges. The label d_{ij} represents the path length between nodes i and j, which is the distance a PLC signal travels when transmitted from i to j.

The main objective of this work is to recover the graph (as in Figure 1(b)) and thus the grid topology (as in Figure 1(a)) based on distance information between the leaf nodes in the tree. Inference of a grid topology is deemed successful if the connection of leaf nodes through branch nodes as well as the distances between all node pairs (leaf and branch nodes) are faithfully reconstructed. For measuring the distances between outer vertices, the nodes transmit and receive PLC signals as described in the next section. These measurements are then processed as discussed in Section IV.

III. PLC-based Ranging

In this section, we address the problem of distance measurement using PLC signaling, i.e., PLC-based ranging. We first briefly review the two-way ranging methodology, which is required to compensate for the clock offset between different modems. Two-way ranging is based on time-of-arrival (ToA) estimation. We discuss a traditional ToA estimation method using signal-energy detection, before introducing a new ToA estimation method which makes use of the PLC signal propagation model. We finally also summarize assumptions for and limitations of the discussed ranging methods.

A. Two-Way Ranging

The local clock time of a modem can be modelled as $C(t) = (1+\delta)t + \mu$, where t denotes the true time and δ and μ are the clock drift and offset, respectively. Two-way ranging allows us to determine the distance between two modems i and j regardless of the offset μ, cf. e.g. [33]. Denoting the local clock times by $C_i(t)$ and $C_j(t)$, the two-way ranging signal exchange between modems i and j with distance d_{ij} is illustrated in Figure 2. At time t_1, i sends a message to j, which it receives at time t_2. Modem j returns a message to i at time t_3, after a pre-defined response delay τ_d, which modem i receives at time t_4. We can write the relationships between the transmission and reception times as

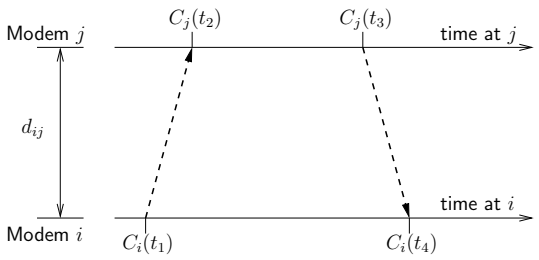

Fig. 2. Two-way ranging between modems i and j with distance d_{ij} and local clock times $C_i(t)$ and $C_j(t)$.

$$
\begin{aligned}
C_j(t_3) - C_j(t_2) &= \tau_\mathrm{d} && (1)\\
t_2 - t_1 &= d_{ij}/v_\mathrm{p} + \varepsilon_{\mathrm{ToA},1} && (2)\\
t_3 - t_2 &= (C_j(t_3) - C_j(t_2))/(1+\delta_j) && (3)\\
t_4 - t_3 &= d_{ij}/v_\mathrm{p} + \varepsilon_{\mathrm{ToA},2}\ , && (4)
\end{aligned}
$$

where v_p is the speed of signal propagation and $\varepsilon_{\mathrm{ToA},1}$ and $\varepsilon_{\mathrm{ToA},2}$ are the errors in estimating the ToA at modem j and i, respectively (measured with respect to the true time t). The estimate $\hat{d}_{ij}$ of the actual distance d_{ij} is then obtained from

$$
\begin{aligned}
\hat{d}_{ij} &= v_\mathrm{p}\frac{C_i(t_4) - C_i(t_1) - \tau_\mathrm{d}}{2}\\
&= (1+\delta_i)\left(d_{ij} + v_\mathrm{p}\frac{\varepsilon_{\mathrm{ToA},1} + \varepsilon_{\mathrm{ToA},2}}{2}\right)\\
&\quad + v_\mathrm{p}\frac{(\delta_i - \delta_j)\tau_\mathrm{d}}{2(1+\delta_j)}\ .
\end{aligned} \qquad (5)
$$

In Section V-A, we present a numerical evaluation of the effect of the clock drift δ on ranging accuracy based on (5), which shows that for typical PLC modems clock drift is not the limiting factor for ranging accuracy down to the meter level. Hence, we neglect the clock drift in the following and turn to the methods of ToA estimation, which will lead to different ToA errors ε_ToA and thus ranging errors $\hat{d}_{ij} - d_{ij}$.

B. Energy-detection ToA Estimation

One of the most common and well researched ToA estimation techniques is based on measuring the energy of the received signal. In essence, the short-term energy measurement is compared to a threshold to determine the ToA, cf. e.g. [33], [34]. Energy-based detection has the advantage of simplicity and robustness to nuisance effects such as multipath propagation. It has recently also been adopted in [18] for ToA estimation in PLC systems.

The main steps of this method are as follows. The transmitter sends a sensing signal $s(t)$, which after convolution with the channel impulse response $h(t)$ is filtered with a zonal bandpass filter for noise limitation at the receiver. This filter could be a matched filter for the transmitted signal [18] or

an approximation of it. The filtered received signal $r(t)$ is then integrated over an interval $T_{\rm int}$. Based on the sampled integrator output

$$q_k = \int_{kT_{\rm int}}^{(k+1)T_{\rm int}} |r(t)|^2 {\rm d}t \ , \quad k = 0, 1, \ldots, K-1 \ , \qquad (6)$$

where $KT_{\rm int}$ is the observation interval, the ToA can be estimated using a number of maximization or thresholding criteria [33]. Following [18], we use the test

$$\hat{t}_{\rm ToA} = T_{\rm int} \underset{k=0,\ldots,K-1}{\rm argmin} \left\{ \frac{q_k - q_{\rm min}}{q_{\rm max} - q_{\rm min}} > \lambda \right\} \qquad (7)$$

to determine the estimated ToA, where $q_{\rm min} = \min_k q_k$ and $q_{\rm max} = \max_k q_k$.

C. Model-based ToA Estimation

We now propose a new ToA estimation method for PLC which makes use of the two-conductor transmission line modelling of propagation over power lines [3, Ch. 2].

1) Propagation Model: Signal propagation over a power line is determined by (i) the propagation constant

$$\gamma(f) = \alpha(f) + {\rm j}\beta(f) \ , \qquad (8)$$

where $\alpha(f)$ and $\beta(f)$ are the frequency (f) dependent attenuation and propagation constant, respectively, and (ii) the reflections and transmissions at discontinuities, such as branch points. These are represented through transmission and reflection coefficient $\Gamma(f)$ and $T(f)$, respectively, defined as

$$\Gamma(f) = \frac{Z(f) - Z_0(f)}{Z(f) + Z_0(f)} \qquad (9)$$

and $T(f) = 1 + \Gamma(f)$, where $Z_0(f)$ is the characteristic impedance of the line and $Z(f)$ is the impedance at the point of discontinuity.

In the following, we use m as path index for a PLC signal, where $m = 1$ corresponds to the direct propagation path, and $m > 1$ corresponds to a signal path including reflections. d_m represents the distance of the m-th path. The sequence of reflection and transmission coefficients along the m-th path can be expressed as $\Gamma_n^m(f)$, $n = 1, \ldots, N_\Gamma(m)$, and $T_n^m(f)$, $n = 1 \ldots, N_T(m)$, respectively, where $N_\Gamma(m)$ and $N_T(m)$ represent the number of reflections and transmissions along the m-th path, respectively. Then, we can write the transfer function of a power line channel as (cf. [35], [3, Ch. 2])

$$\begin{aligned} H(f) &= \sum_{m=1}^{\infty} \left(\prod_{n=1}^{N_\Gamma(m)} \Gamma_n^m(f) \right) \left(\prod_{n=1}^{N_T(m)} T_n^m(f) \right) {\rm e}^{-d_m \gamma(f)} \\ &\triangleq \sum_{m=1}^{\infty} A_m(f) {\rm e}^{-d_m \gamma(f)} \ . \end{aligned} \qquad (10)$$

For compactness, in (10), we aggregated the products of the reflection and transmission coefficients for the m-th reflection in the term $A_m(f)$.

To formulate the parametric ToA estimation method, we need to invoke the following assumptions for the propagation model. First, we assume that $\alpha(f)$ and $\beta(f)$ are well approximated as linear functions of the frequency:[2]

$$\alpha(f) = a \cdot f \ , \quad \beta(f) = \frac{2\pi}{v_{\rm p}} f \ . \qquad (11)$$

These approximations are a good match for weakly lossy lines and naturally tighter for smaller frequency range $f_{\rm min} \leq f \leq f_{\rm max}$. Second, we approximate the coefficients $A_m(f)$ as constants over the frequency band used for ranging. Again, this approximation becomes tighter for smaller signal bandwidth $f_{\rm max} - f_{\rm min}$. Third, we truncate the number of paths to $N_{\rm p}$. This is not a severe approximation, as the contributions from paths with larger distances d_m passing more discontinuities usually undergo significantly stronger attenuation. Applying the approximations to (10), we obtain

$$H(f) = \sum_{m=1}^{N_{\rm p}} A_m {\rm e}^{-a d_m f} {\rm e}^{-{\rm j}\frac{2\pi}{v_{\rm p}} d_m f} \ . \qquad (12)$$

2) ToA Measurements and Algorithm: Given (12), we are ready to present the new model-based ToA estimation method. Assuming OFDM transmission as widely used and standardized for PLC, e.g. [8], we can measure samples $H_k = H(f_k){\rm e}^{{\rm j}2\pi(t_{\rm W} - t_{\rm T})f_k}$ of the "time-shifted" transfer function $H(f){\rm e}^{{\rm j}2\pi(t_{\rm W} - t_{\rm T})f}$ at frequencies $f_k = f_{\rm min} + k\Delta f$, $k = 0, 1, \ldots, N_{\rm f} - 1$, where $N_{\rm f} = (f_{\rm max} - f_{\rm min})/\Delta f + 1$. The rotation term results from the difference between the time $t_{\rm T}$ when the OFDM symbol is transmitted and the time $t_{\rm W}$ when the receiver observation window for the OFDM symbol starts. Introducing the signal propagation time for the m-th path $t_m = d_m / v_{\rm p}$, the samples can be written as

$$\begin{aligned} H_k &= \sum_{m=1}^{N_{\rm p}} A_m {\rm e}^{-(a + {\rm j}\frac{2\pi}{v_{\rm p}}) d_m f_{\rm min}} {\rm e}^{-(a d_m + {\rm j}2\pi(t_m + t_{\rm T} - t_{\rm W}))\Delta f k} \\ &\triangleq \sum_{m=1}^{N_{\rm p}} B_m z_m^k \ , \end{aligned} \qquad (13)$$

where we defined $B_m = A_m {\rm e}^{-(a + {\rm j}\frac{2\pi}{v_{\rm p}}) d_m f_{\rm min}}$ and the complex exponential $z_m = {\rm e}^{-(a d_m + {\rm j}2\pi(t_m + t_{\rm T} - t_{\rm W}))\Delta f}$.

The ToA of the transmitted signal is $t_1 + t_{\rm T}$. Hence, based on (13) the problem of estimating the ToA can be considered as a parameter-estimation problem of superimposed exponential signals. Numerous methods for solving this problem have been proposed in the literature, including maximum likelihood [36], linear-prediction based [37], [38], matrix-pencil [39], and subspace [40] methods. We have found that the subspace method produces very accurate results, and its main steps are described in the following algorithm (see [40] for further details).

[2] Frequency-independent offsets can be assigned to $A_m(f)$.

Algorithm: Subspace method for ToA estimation

1: Construct an $M \times (N_\mathrm{f} - M)$ matrix

$$\boldsymbol{H} = \begin{bmatrix} H_0 & H_1 & \cdots & H_{N_\mathrm{f}-M-1} \\ H_1 & H_2 & \cdots & H_{N_\mathrm{f}-M} \\ \vdots & \vdots & & \\ H_{M-1} & H_M & \cdots & H_{N_\mathrm{f}-1} \end{bmatrix} \quad (14)$$

where $M, N_\mathrm{f} - M > N_\mathrm{p}$.

2: Compute the singular value decomposition $\boldsymbol{H} = \boldsymbol{U}\boldsymbol{S}\boldsymbol{V}^H$

3: Find the largest S singular values and the corresponding left and right singular vectors $\boldsymbol{U}_\mathrm{s}$ and $\boldsymbol{V}_\mathrm{s}$, respectively.

4: Compute estimates $\hat{z}_m$ for z_m in (13) as the eigenvalues of the matrix $\boldsymbol{Z} = \underline{\boldsymbol{U}_\mathrm{s}}^{+}\overline{\boldsymbol{U}_\mathrm{s}}$, where $(.)^+$ represents the pseudo-inverse, and $\overline{(.)}$ and $\underline{(.)}$ denote the operation of deleting the first and the last row, respectively.

The value of S used in the subspace-method algorithm ideally coincides with the number N_p of significant echoes, which however is unknown. Different methods have been devised to determine N_p, including the use of information-theoretic criteria [41], [42]. However, since we are eventually only interested in an estimate for t_1 and thus z_1, the used value for N_p is not particularly critical. Using the number of singular values of $\boldsymbol{H}$ defined in (14) that are significantly above the variance of the measurement noise when estimating H_k in (13) turned out to deliver a suitable choice for S.

Given $\hat{z}_1$ from the subspace-method algorithm, we can compute the ToA estimate as

$$\hat{t}_\mathrm{ToA} = \frac{\arg\{z_1\}}{2\pi\Delta f} + t_\mathrm{W} \; . \quad (15)$$

D. Remarks on Assumptions and Limitations

Before using the presented ranging methodology for topology estimation via tomography, we would like to summarize the assumptions we made in the previous derivations, some of which were made tacitly.

1) We estimate distance based on signal delay, relating these two quantities via the speed of propagation v_p, cf. (5). Hence, we require that there is only one value for v_p. Since however the power grid may include different cable types, different values for v_p may occur along the PLC signal path. For example, for the weakly lossy two-conductor line model with homogeneous dielectric, we have
$$v_\mathrm{p} = 1/\sqrt{\mu_0 \varepsilon_0 \varepsilon_\mathrm{r}} \; , \quad (16)$$
where the parameters μ_0, ε_0, and ε_r are the vacuum permeability and permittivity, and the relative permittivity of the insulation between the conductors, respectively. Hence, cables with different insulation material will result in different speeds of signal propagation, which would affect the ranging accuracy.
2) While our derivations start with a time-invariant channel model, e.g. (10), the PLC channel has been shown to be time varying in many cases. In particular, time variations periodic with the mains frequency (i.e., 50 Hz or 60 Hz) have been observed, e.g. [3, Section 2.5.3], [43]. However, the channel changes only very slowly during the transmission of a ranging message, which would typically be shorter than those used for broadband PLC data transmission. For example, [3, Section 2.5.3], [43] mention that the channel coherence time is no smaller than 600 μs, while the OFDM-symbol length for broadband PLC according to IEEE 1901 is about 50 μs. Furthermore, [44] shows that signal-to-distortion power ratios due to temporal changes of the channel are in excess of 55 dB for typical broadband PLC parameters. Hence, the effect of time variations for ranging should be negligible.
3) In the case of model-based ranging, deviations from the model approximation (12) will deteriorate accuracy. This includes the above-mentioned variation in propagation speed, the variations of load impedances over frequency, and the approximation in (11).

IV. PLC Network Tomography

Applying the tree model from Section II, we are now putting the ranging algorithms from the previous section to use for the purpose of topology inference.

The first step of inference is to perform ranging between all PLC modems, which are located at the leaves of the network tree. The measured distances are communicated to a centralized node, e.g., the master node in a PLC network, which then runs a tree-estimation algorithm with these distances as the input. At this point, we make use of the fact that end-to-end distance measurements between leaf nodes uniquely define the tree connecting them. In particular, our topology-inference problem is alike the phylogenetic-tree inference problem in evolutionary biology, for which the neighbor-joining algorithm (NJA) from [46] is widely used. We apply a variant of the NJA, the rooted neighbor-joining algorithm (RNJA), that was recently developed in [45].

Table I shows the pseudo-code of the RNJA that we use. First, the RNJA defines a root node. Considering the remaining set of leaf nodes, based on the measured distances it finds two leaf nodes which are likely connected to the same internal node. These leaf nodes and the edges to the new internal node are stored as part of the tree structure, and the new internal node replaces the original leaf nodes in the next iteration. The process is reiterated until only one leaf node is left.

We note that the key for the applicability of the RNJA (or the original NJA) is the additivity of the distances d_{ij}, i.e., $d_{ik} = d_{ij} + d_{jk}$, if node j is on the path from node i to node k. For the inference problem at hand, additivity follows naturally as the d_{ij} are indeed physical distances. Furthermore, the RNJA inherits a remarkable convergence property from the NJA. It returns the correct tree topology if the measured distances $\hat{d}_{ij}$ deviate from the true distances d_{ij}, $\forall i, j \in \mathcal{V}$, by less than half the minimum edge length in the tree, cf. [45]. That is, if d_min is the shortest link between two nodes, then measurement errors up to $d_\mathrm{min}/2$ can be tolerated while still retrieving a result consistent with the true tree topology.

TABLE I
PSEUDO-CODE FOR THE ROOTED NEIGHBOR-JOINING ALGORITHM (FOLLOWING [45]).

Input:	Measured distances $\hat{d}_{ij}$, number of leaf nodes K	
Initialize:	root node $s = 1$,	
	set of leaf nodes of inspected tree $\mathcal{D} = \{2, \ldots, K\}$	
	set of nodes of output tree $\mathcal{V} = \{s\}$	
	set of edges of output tree $\mathcal{E} = \emptyset$	
	Enumerator for new nodes $f = K$	
Start:	**While** $(\lvert\mathcal{D}\rvert > 1)$	% Go through all leaf nodes
	For $i, j \in \mathcal{D}$	% Compute distance between root node and nearest
	$\hat{q}_{ij} = \frac{1}{2}(\hat{d}_{si} + \hat{d}_{sj} - \hat{d}_{ij})$	% common ancestor node of i and j
	end	
	$(i^*, j^*) = \mathrm{argmax}_{(i,j)}\{\hat{q}_{ij}\}$	% Nodes that maximize distance are neighbors
	$f := f + 1$	% Add a new node f, the ancestor of i^* and j^*
	$\mathcal{D} := \mathcal{D} \setminus \{i^*, j^*\}$	% Prune tree (remove i^* and j^* from the list of leaf nodes)
	$\mathcal{V} := \mathcal{V} \cup \{i^*, j^*\}$	% Add i^* and j^* to the list of tree nodes
	$\mathcal{E} := \mathcal{E} \cup \{(f, i^*), (f, j^*)\}$	% Add (i^*, j^*) to the list of tree edges
	$\hat{d}_{sf} = \hat{q}_{i^*j^*}$, $\hat{d}_{fi^*} = \hat{d}_{si^*} - \hat{q}_{i^*j^*}$, $\hat{d}_{fj^*} = \hat{d}_{sj^*} - \hat{q}_{i^*j^*}$	% Compute distances from s, i^*, j^* to new node f
	For $k \in \mathcal{D}$	% Compute distance from leaf nodes to new node f
	$\hat{d}_{kf} = \frac{1}{2}(\hat{d}_{ki^*} - \hat{d}_{fi^*}) + \frac{1}{2}(\hat{d}_{kj^*} - \hat{d}_{fj^*})$, $\hat{q}_{kf} = \frac{1}{2}(\hat{q}_{ki^*} + \hat{q}_{fj^*})$	
	end	
	$\mathcal{D} := \mathcal{D} \cup f$	% New node becomes leaf node of pruned inspected tree
	end	% End while
End:	$\mathcal{V} := \mathcal{V} \cup \mathcal{D}$, $\mathcal{E} := \mathcal{E} \cup (s, \mathcal{D})$	% Complete output tree
Output:	Reconstructed tree: nodes $\mathcal{V}$ and edges $\mathcal{E}$	

Finally, we note that the RNJA in Table I is applicable to binary trees. As shown in [45], it can be extended to general trees with only a slight modification to the pseudo-code in Table I. The price for this extension is some loss in robustness to measurement errors. Therefore, the RNJA in Table I is preferable if the underlying PLC topology is a-priori known to fit the binary-tree model.

We observe that RNJA in Table I is a batch algorithm. Ranging measurements between all pairs of nodes need to be provided before the algorithm can start. An interesting alternative is the sequential version of the RNJA presented in [47, Section VI], which constructs the topology tree incrementally. This reduces the number of ranging measurements and can facilitate topology reconstruction for dynamic networks, where nodes (PLC modems) join. A variation of the method may also be applicable to larger PLC networks with no direct link between all pairs of nodes (cf. also [48] for this problem).

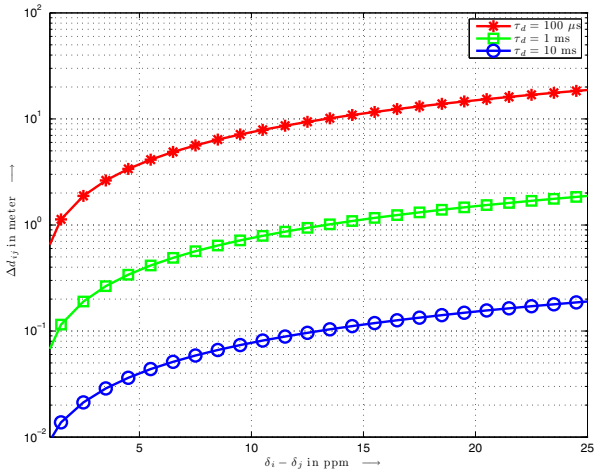

Fig. 3. Estimation error $\Delta d_{ij} = \hat{d}_{ij} - d_{ij}$ as function of $\delta_i - \delta_j$ for $\delta_i = 25$ ppm, processing delays $\tau_\mathrm{d} = [0.1, 1, 10]$ ms, and $d_{ij} = 100$ m.

V. PERFORMANCE EVALUATION

In this section, we assess the performance of the proposed PLC-based power grid tomography method. We first consider the accuracy of PLC-based ranging. To this end, in Section V-A, we establish the effect of clock drift between PLC modems on ranging accuracy. This is followed by a detailed quantitative performance comparison of energy-detection and model-based ranging in Section V-B. Finally, Section V-C presents the numerical analysis of tomography with the RNJA.

A. Effect of Clock Drift for PLC Systems

To highlight the effect of clock drift on two-way ranging, let us evaluate expression (5) under the assumption of perfect ToA estimation. To this end, Figure 3 shows the distance estimation error $\Delta d_{ij} = \hat{d}_{ij} - d_{ij}$ as a function of $\delta_i - \delta_j$ for $\delta_i = 25$ ppm and processing delays $\tau_\mathrm{d} = [0.1, 1, 10]$ ms. We observe that for processing delays of $\tau_\mathrm{d} = 0.1$ ms and $\tau_\mathrm{d} = 1$ ms, the estimation error is less than 0.2 m and 2 m, respectively, even for a relative clock drift of 25 ppm. For a fairly long delay of $\tau_\mathrm{d} = 10$ ms, a relative clock drift of less than 5 ppm is desirable to keep the estimation error low. We note that the results in Figure 3 are rather independent of d_{ij} as the second term in (5) dominates for $\varepsilon_{\mathrm{ToA},1} = \varepsilon_{\mathrm{ToA},2} = 0$. Since for broadband PLC modems clock tolerances of ± 25 ppm and relative clock drifts within ± 1 ppm after frequency correction are considered [8], we conclude from the analysis in this section that clock drift is not the limiting factor for ranging accuracy down to the meter level. Hence, for the following discussion, we neglect the clock drift.

B. Ranging Accuracy

We now apply the ranging algorithms introduced in Section III to specific PLC network examples.

1) Topologies and Channel Parameters: We consider the power line topologies shown in Figures 4 and 5. Both represent parts of an LV distribution grid served by a transformer, modeled by the impedance Z_s, and supplying loads, which

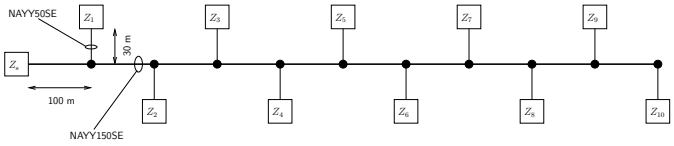

Fig. 4. Topology 1. Power line network with 11 nodes, located at transformer with impedance $Z_{\rm s}$ and at loads (e.g., house connection points) with impedances Z_i, mimicking part of a low-voltage distribution grid as in [3, Figure 2.16].

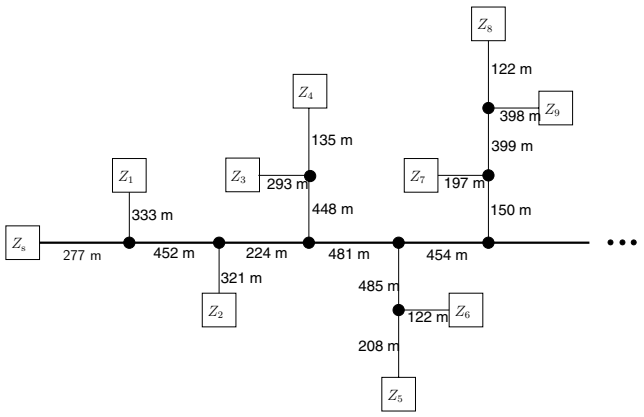

Fig. 5. Topology 2 from Figure 8 in [32]. PLC nodes are located at the loads with impedances Z_i and the transformer with impedance $Z_{\rm s}$. Shown are 9 loads of the entire topology, which includes 20 loads.

could for example be houses, modeled by impedances Z_i. The topology in Figure 4 closely resembles the example of a European power distribution network in a residential area introduced in [3, Figure 2.16]. The topology in Figure 5 is taken from [32, Figure 8]. It includes a total of 20 loads, of which nine are shown in Figure 5. The PLC network is composed of nodes located at the transformer and at the loads. This could be a PLC network for an advanced metering infrastructure, enabling communication between the meters at the consumers and the data concentrator point at the transformer station.

To compute the transfer functions $H(f)$ (10) based on the propagation constants $\gamma(f)$ (8) and reflection and transmission coefficients $\Gamma(f)$ at branch points according to (9), we need to make specific assumptions about power cables and signal injections. To this end, we consider popular 4-conductor cables NAYY150SE and NAYY50SE with signal coupling between two phases and the neutral conductor as described in [3, Section 2.3.3.1]. For this case, making a two-conductor equivalent approximation (see [3, Section 2.3.3.1]), the transmission line parameters can be approximated as

$$\begin{aligned} R' = \sqrt{\rho\pi f\mu_0/r^2},\, G' = 2\pi f C' \tan(\delta_{\rm C}), \\ L' = \mu_0\vartheta/(2r),\, C' = 2\varepsilon_0\varepsilon_{\rm r} r/\vartheta\ , \end{aligned} \tag{17}$$

from which we can compute the characteristic impedance and propagation constant as

$$Z_0(f) = \sqrt{\frac{R' + {\rm j}2\pi f L'}{G' + {\rm j}2\pi f C'}} \tag{18}$$

$$\gamma(f) = \sqrt{(R' + {\rm j}2\pi f L')(G' + {\rm j}2\pi f C')}\ . \tag{19}$$

In (17), the parameters $\tan(\delta_{\rm C})$, ρ, r and ϑ are the dielectric loss angle of the insulation, the specific resistance of the conductor, the radius of the cable and the thickness of the insulation, respectively, cf. [3, Fig. 2.26 and Section 2.3.3.1]. Consulting [49], we have $r = 15.6$ mm, $\vartheta = 3.6$ mm and $r = 9.4$ mm, $\vartheta = 2.8$ mm for NAYY150SE and NAYY50SE, respectively. Furthermore, $\rho = 2.8 \cdot 10^{-8}\,\Omega$m (for aluminum), and we assume that $\epsilon_r = 4$ and $\tan(\delta_{\rm C}) = 0.01$ [3, Section 2.3.3.1].

While the cable type NAYY150SE is used for all lines of Topology 2 shown in Figure 5, for Topology 1 we assume that the main power line is an NAYY150SE cable and the cables branching off (e.g., to connect houses) are of type NAYY50SE, as indicated in Figure 4. NAYY50SE has a smaller gauge than NAYY150SE, and using both types for Topology 1 includes the effects of impedance mismatch of cables. However, the phase velocity (16) is $v_{\rm p} = 1.5 \cdot 10^8$ m/s and the same for both cable types, as we assume the same type of insulation.

We further need to specify the values of the impedances $Z_{\rm s}$ and Z_i of the transformer and loads shown in Figures 4 and 5. For the former, we apply the three-element circuit model from [4]. For the latter and Topology 2, we use the values given in [32, Figure 8]. For Topology 1, we consider two cases. In the first case, $Z_i = 5\ \Omega$, $i = 1, \ldots, 10$. In the second case, the impedance values are generated randomly according to a uniform distribution in $([0, 5] + {\rm j}[-5, 5])\ \Omega$. This is done to specifically investigate the effect of low impedance values, which affect the channel gain for PLC. The impedance of PLC modems is set to $50\ \Omega$, which is typical when in receiving mode and applied in parallel to $Z_{\rm s}$ and Z_i.

Finally, we assume that PLC modems transmit with a power spectral density of -55 dBm/Hz [8] and that the receiver-side noise power spectral density (PSD) is -110 dBm/Hz, which is a relatively high background noise PSD. Of course, impulse noise is a major impairment in PLC channels. We do not include it here, for simplicity, but also because it will likely completely distort the transmitted PLC ranging signal, causing a retransmission of the same.

2) Energy-detection (ED) and Model-based (MB) Ranging Parameters: In the following, we refer to two-way ranging using energy-detection (ED) ToA estimation from Section III-B and model-based (MB) ToA estimation from Section III-C as ED and MB ranging, respectively. We assume that a broadband PLC signal in the frequency band from 2 MHz to 28 MHz (cf. [8]) is transmitted for ED ranging. This leads to a temporal resolution on the order of 40 ns, corresponding to a spatial resolution of about 5 m using $v_{\rm p}$ given above. We set the integration interval $T_{\rm int}$used in (6) and (7) equal to the sampling interval 1/26 μs. For the threshold λ we use 0.1 and 0.8, respectively. We found empirically that these values lead to favorable ED accuracy, cf. also [18].

For the new MB ranging we use $f_{\min} = 2$ MHz and $f_{\max} = 8$ MHz. This, compared to ED ranging, reduced bandwidth (i) is used to demonstrate the super-resolution capabilities of MB ranging, (ii) achieves an increased signal-to-noise ratio (SNR) since cable attenuation increases with frequency, and (iii) makes the assumption of frequency-independent load impedances more realistic. Furthermore, while $f_{\max} = 8$ MHz is the default value, we also show one set of results for $f_{\max} \in \{3, 4, \ldots, 8\}$ MHz.

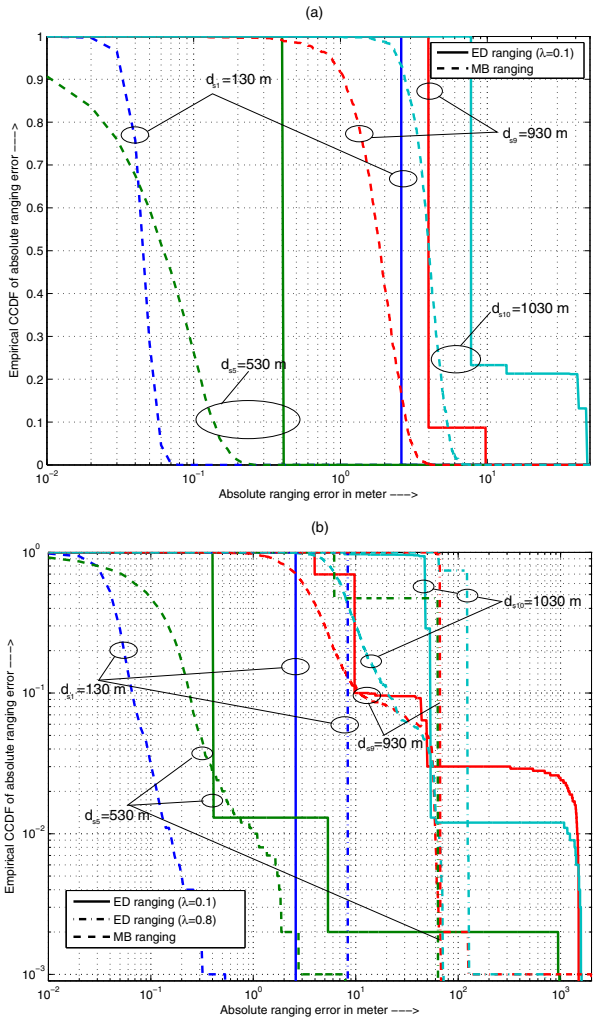

Fig. 6. Empirical CCDF of absolute ranging error for different links from node s (transformer) to nodes i at loads Z_i with distances $d_{\mathrm{s}i}$ from Topology 1. Solid lines: Energy detection (ED) ranging with $\lambda = 0.1$. Dash-dotted lines: ED ranging with $\lambda = 0.8$. Dashed lines: Model-based (MB) ranging. (a): $Z_i = 5\ \Omega$, $i = 1, \ldots, 10$. (b): Z_i sampled uniformly random from $([0,5] + \mathrm{j}[-5,5])\ \Omega$.

3) Results: Denoting the distance between two nodes as d_{ij} and the estimated distance as $\hat{d}_{ij}$, the following results consider the absolute ranging error

$$e_{ij} = |d_{ij} - \hat{d}_{ij}| \,. \tag{20}$$

We first consider Topology 1. Figure 6 shows the empirical complementary cumulative density function (CCDF) of the absolute ranging error from (20) for four different links and thus distances ('s' refers to the node at the transformer with impedance Z_{s}). The subfigures (a) and (b) assume fixed and randomly generated load impedances, respectively. A total of 1000 ranging measurements with different channel and noise realizations were performed for the results. Considering the case of fixed load impedances, we observe that MB ranging achieves good ranging accuracy. The ranging errors are less than 6 m for all channel realization. For the shorter links of lengths 130 m and 530 m, accuracy is in the submeter range. In the case of ED ranging (using $\lambda = 0.1$), the error exceeds 10 m in a few cases for the longest link of length 1030 m. Clearly, ranging accuracy generally decreases with increasing

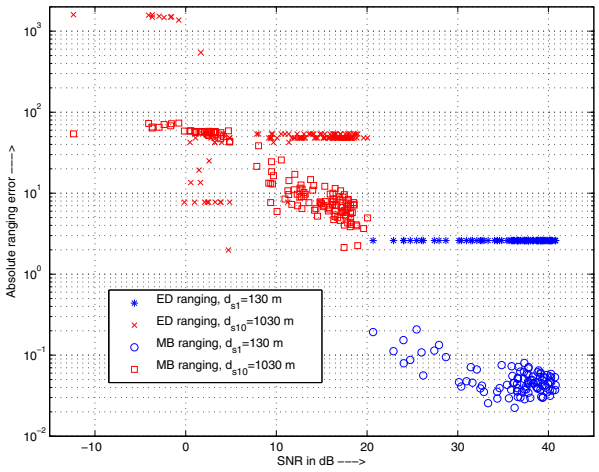

Fig. 7. Scatter plot of absolute ranging error as function of average channel SNR for the frequency range from 2 MHz to 8 MHz. Links from node s (transformer) to node 1 and node s to node 10 with distances $d_{\mathrm{s}1}$ and $d_{\mathrm{s}10}$, respectively, from Topology 1, and randomly generated loads from $([0,5] + \mathrm{j}[-5,5])\ \Omega$.

link distances due to stronger signal attenuation and thus lower SNR at the receiver side. When replacing the fixed impedances of 5 Ω (Figure 6(a)) with random impedances in the range of $([0,5] + \mathrm{j}[-5,5])\ \Omega$ (Figure 6(b)), we note a degradation in accuracy. This is due to the larger signal losses at low impedances, which manifests in a smaller transmission gain $|H(f)|$ and thus SNR. As can be seen from Figure 6(b), 10% of the errors exceed 10 m (930 m link) and 20 m (1030 m link), respectively, also for MB ranging. However, it still remains the preferable ranging mode compared to ED ranging. For the latter, we show the results for both the threshold values $\lambda = 0.1$ and $\lambda = 0.8$. Using the larger threshold leads to a degradation in ranging accuracy but avoids the large outliers.

The correlation of ranging accuracy with SNR is highlighted in Figure 7. We show a scatter plot of the absolute ranging error e_{ij} for $(i,j) \in \{(\mathrm{s},1),(\mathrm{s},10)\}$ and the average SNR at the receiver side in the frequency band from 2 MHz to 8 MHz, which is used for MB ranging. The shortest and longest link from Topology 1, which are from transformer node s to nodes 1 and 10 with distances $d_{\mathrm{s}1} = 130$ m and $d_{\mathrm{s}10} = 1030$ m, respectively, the scenario with randomly generated loads (Figure 6(b)), and ED ranging with $\lambda = 0.1$ are considered. For the short link of $d_{\mathrm{s}1} = 130$ we observe consistently high SNRs of above 20 dB, which enables accurate ranging with about 2 m and submeter accuracy for ED and MB ranging, respectively. We note that the ranging error e_{ij} for ED ranging is identical for all test runs. This is because the error is dominated by the resolution limit of ED, which follows from the 26 MHz signal bandwidth. In contrast to this, MB ranging is a super-resolution technique, whose performance is dominated by noise. Hence, a cloud of markers can be seen for MB ranging in Figure 7. Considering the long link of $d_{\mathrm{s}10} = 1030$ m, SNRs as low as -11 dB occur. We observe that ranging accuracy deteriorates with decreasing SNR. The outliers with $e_{\mathrm{s}10} > 1000$ m for ED ranging could be suppressed with adapting the threshold λ, see Figure 6(b). MB ranging proves to be relatively robust to low SNRs.

TABLE II
AVERAGE ABSOLUTE ESTIMATION ERROR FOR ED AND MB RANGING AND LINKS IN TOPOLOGY 1. FIXED LOAD IMPEDANCES OF $Z_i = 5\ \Omega$, $i = 1, \ldots, 10$. 's' REFERS TO NODE AT TRANSFORMER.

ED ranging, average error e_{ij} from (20) in meter											
Tx node	Rx node										
	s	1	2	3	4	5	6	7	8	9	10
s	-	2.6	6.4	1.4	3.4	0.4	1.6	2.2	5.5	4.5	15.3
1	2.6	-	1.4	5.2	2.6	2.6	1.8	2.8	1.3	2.4	3.8
2	6.4	1.4	-	1.4	5.2	2.6	3.6	2.8	2.9	1.3	4.6
3	1.4	5.2	1.4	-	1.4	5.2	2.6	3.7	3.2	3.0	1.0
4	3.4	2.6	5.2	1.4	-	1.4	5.2	2.6	3.8	4.1	2.8
5	0.4	2.6	2.6	5.2	1.4	-	1.4	5.2	2.6	4.3	0.8
6	1.6	2.0	3.7	2.6	5.2	1.4	-	1.4	5.2	2.6	1.4
7	2.2	2.8	2.9	3.8	2.6	5.2	1.4	-	1.4	5.2	2.6
8	4.5	1.3	2.9	3.2	3.9	2.6	5.2	1.4	-	1.4	5.2
9	4.0	2.5	1.3	2.9	4.1	4.3	2.6	5.2	1.4	-	1.4
10	9.6	4.5	4.8	1.0	2.8	0.8	1.3	2.6	5.2	1.4	-

MB ranging, average error e_{ij} from (20) in meter											
Tx node	Rx node										
	s	1	2	3	4	5	6	7	8	9	10
s	-	0.1	0.0	0.0	0.1	0.1	0.5	0.8	1.1	1.9	4.1
1	0.0	-	0.1	0.1	0.1	0.1	0.2	0.2	1.6	2.8	0.9
2	0.0	0.1	-	0.1	0.1	0.1	0.1	0.1	0.3	1.3	3.2
3	0.0	0.1	0.1	-	0.1	0.1	0.1	0.1	0.1	0.4	0.6
4	0.0	0.1	0.2	0.1	-	0.1	0.1	0.1	0.3	0.1	0.5
5	0.1	0.1	0.1	0.1	0.1	-	0.1	0.2	0.1	0.1	0.1
6	0.2	0.2	0.1	0.1	0.1	0.1	-	0.1	0.1	0.1	0.0
7	0.5	0.2	0.1	0.1	0.1	0.2	0.1	-	0.1	0.1	0.1
8	1.6	1.6	0.4	0.1	0.3	0.1	0.1	0.1	-	0.0	0.0
9	1.4	2.8	1.3	0.3	0.1	0.1	0.1	0.1	0.0	-	0.1
10	3.0	0.7	2.7	0.9	0.3	0.1	0.1	0.1	0.0	0.0	-

Table II summarizes the accuracy of ED ($\lambda = 0.1$) and MB ranging in terms of the average absolute ranging error e_{ij} for the 1000 ranging measurements and the different links of Topology 1 in the fixed-impedance case. We show the error corresponding to one-way ToA estimation. The error for two-way ranging between modems i and j is the mean of the errors for $i \to j$ and $j \to i$ ToA estimation (see (5)). We observe the following trends. (i) MB ranging is more accurate than ED ranging, often achieving submeter precision. (ii) Ranging accuracy decreases with distance. (iii) Overall accuracy is high enough to support tomography using the RNJA from Table I, which requires that the error is less than half the minimal node-to-node distance. (iv) One-way ranging errors are not symmetric. This is due to the non-symmetry of the transfer function (10) of the power line channel that we consider, which represents the voltage transfer from the coupling point at the input to the decoupling point at the output, mimicking a transmitting modem with a voltage level control.[3] Other factors that could lead to non-symmetric errors are different noise realizations at the two nodes i and j and different clock drifts δ_i and δ_j at the two modems.

[3]In PLC, two different transfer functions are often considered (see Figure 1 and Eqs. (2) and (3) in [26]): $H_1(f) = V_L(f)/V_N(f)$ between the voltage $V_L(f)$ at the load and the voltage $V_N(f)$ at the power line coupling point and $H_2(f) = V_L(f)/V_S(f)$ between the voltage $V_L(f)$ at the load and the voltage $V_S(f)$ of the source. These two are related through the source impedance $Z_S(f)$ and network input impedance $Z_N(f)$ via $H_2(f) = H_1(f)\frac{Z_N(f)}{Z_N(f)+Z_S(f)}$. Transfer function $H_2(f)$ is relevant for modems with fixed $V_S(f)$, while $H_1(f)$ is relevant for modems with an automatic level control that imposes a preferably fixed voltage $V_N(f)$ on the line, e.g. [50]. While the symmetry of $H_2(f)$ has been shown (assuming $Z_S(f) = Z_L(f)$) in [51], $H_1(f)$ is generally not symmetric.

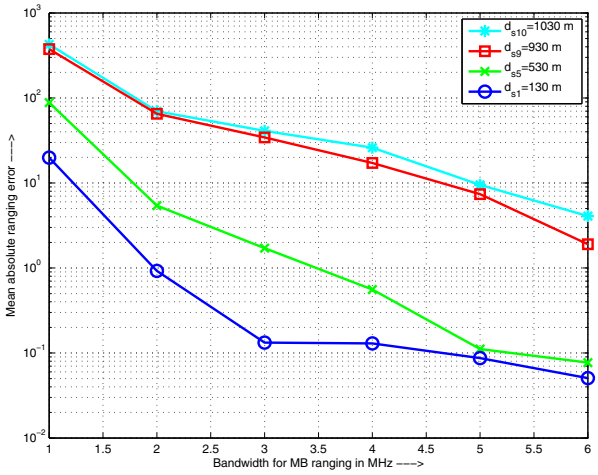

Fig. 8. Average absolute ranging error as function of the bandwidth used for model-based (MB) ranging. Links from node s to nodes 1, 5, 9, and 10 with from Topology 1. Fixed load impedances of $Z_i = 5\ \Omega$, $i = 1, \ldots, 10$.

Next, we illustrate the effect of signal bandwidth on the performance of MB ranging. To this end, Figure 8 shows the average absolute ranging error e_{ij} for the links from node s to nodes $[1, 5, 9, 10]$ for Topology 1 and fixed load impedances. While MB ranging is a super-resolution method whose accuracy is not bounded by the bandwidth of the ranging signal, we observe from the curves in Figure 8 that average accuracy improves with increasing bandwidth. Larger bandwidth helps to improve the condition of matrix $\boldsymbol{H}$ (14) of the sub-space method. This can be seen from the improved accuracy with larger bandwidth also for the short link with distance d_{s1}. Hence, when selecting bandwidth one needs to consider the trade-off between accuracy and validity of the assumption of frequency-independent loads.

Finally, we report ranging results for Topology 2 from Figure 5. Figure 9 shows the empirical CCDF of the absolute ranging error using ED and MB ranging for 1000 experiments, i.e., different noise realizations. For ED ranging, $\lambda = 0.8$ is used as it provided better results than $\lambda = 0.1$. The subfigures (a) and (b) show the results for links from node $i = 1$ and $i = 9$, respectively. Similar to the results for Topology 1 in Figure 6, we observe that ranging accuracy is higher for short links and that MB ranging outperforms ED ranging in terms of accuracy for these links. Different from Figure 6, we note that in some cases the error is larger than 100 m or even 1000 m for MB ranging and that ED with $\lambda = 0.8$ is more robust to these outliers than MB ranging. This occurs for long links like $1 \to 9$ with a distance of 2891 m. Hence, the link distance is much longer than those experienced in Topology 1. However, MB ranging still provides accuracies of $e_{ij} < 10$ m for 90 % and 80 % of the long links ($1 \to 8$, $9 \to 3$) and ($1 \to 9$, $9 \to 1$), respectively. In particular, the shape of the CCDF curve for example for the link $1 \to 9$ indicates that either high accuracy is achieved or, if not, a very large error of about 1000 m occurs. The latter can be relatively easily identified as an outlier through a repeated ranging measurement. Hence, successful tomography is possible even for such an extended topology.

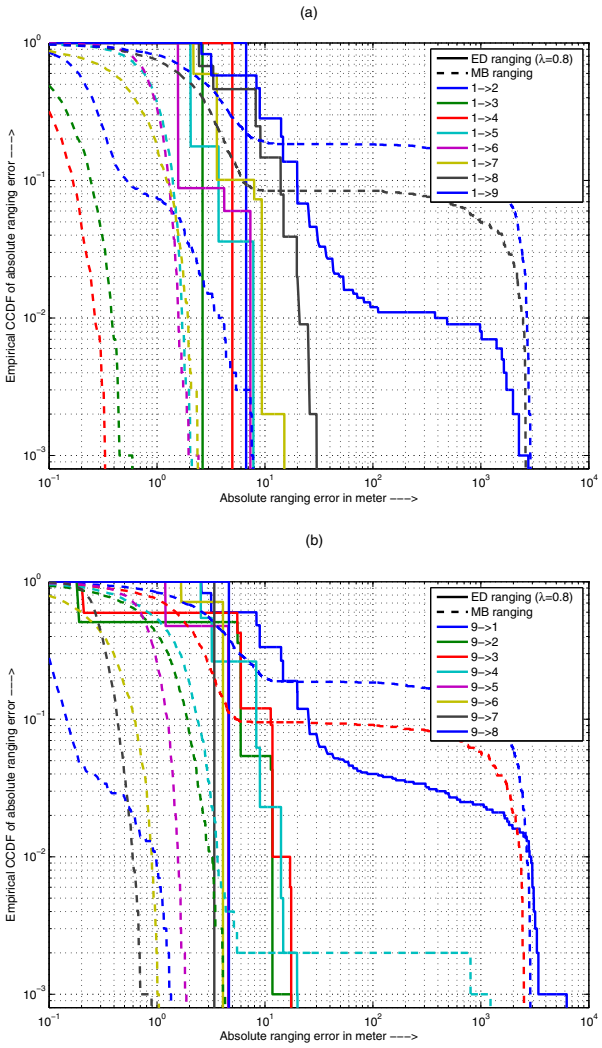

Fig. 9. Empirical CCDF of absolute ranging error for different links from node i to j ('$i \to j$') from Topology 2. Solid lines: Energy detection (ED) ranging. Dashed lines: Model-based (MB) ranging. (a): From node $i = 1$. (b): From node $i = 9$.

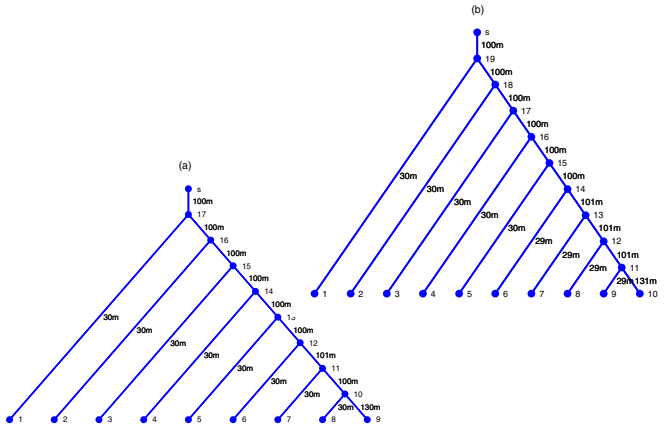

Fig. 10. Example of a reconstructed topology, including distances shown at edges, using the RNJA for Topology 1 with fixed load impedances ($Z_i = 5\ \Omega$, $i = 1, \ldots, 10$). MB ranging measurements are used. (a): Using node-to-node measurements from nodes at transformer and nine loads. Nodes 10 to 17 are created by the RNJA. (b): Using node-to-node measurements from nodes transformer and ten loads. Nodes 11 to 19 are created by the RNJA.

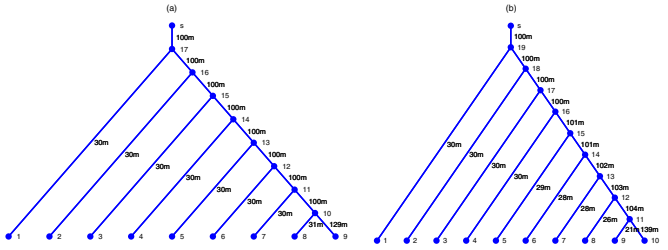

Fig. 11. Example of a reconstructed topology, including distances shown at edges, using the RNJA for Topology 1 with randomly generated load impedances ($Z_i \in ([0, 5] + \mathrm{j}[-5, 5])\ \Omega$, $i = 1, \ldots, 10$). MB ranging measurements are used. (a): Using node-to-node measurements from nodes at transformer and nine loads. Nodes 10 to 17 are created by the RNJA. (b): Using node-to-node measurements from nodes at transformer and ten loads. Nodes 11 to 19 are created by the RNJA.

C. Tomography Results

We now apply the ranging measurements discussed in the previous section as input to the RNJA introduced in Section IV. To illustrate the capability and performance of the proposed tomography method, we first consider samples of reconstructed topologies using MB ranging measurements.

Figure 10 shows two reconstructed topologies for MB ranging measurements of Topology 1 with fixed 5 Ω load impedances. The edges are labeled with the distances as returned by the RNJA (see Table I), and also the internal nodes are created and enumerated by the algorithm. The difference between subfigures (a) and (b) is that the former does not include ranging measurements to and from the node at Z_{10} (see Figure 4). Focusing on Figure 10(a) first, we observe an almost perfect reconstruction of the actual topology. In addition to the correct tree structure, also the distances between leaf and internal nodes have been inferred accurately. Quantizing the distances to meter precision, only the estimated distance for the link between internal nodes 11 and 12 is different from the actual distance by 1 m. Figure 10(b) shows the reconstructed tree for the full Topology 1. Since node 10 increases the size of the topology, which makes ranging less accurate (see Figures 6 and 7), tomography is more challenging compared to the case in Figure 10(a). Still, edge distances are recovered almost perfectly, with errors of at most 1 m. What is interesting to note is that the somewhat less accurate ranging to and from node 10 also affects estimated distances for links not connected to this node. Hence, this indicates that it is better to discard unreliable ranging measurements and limit tomography to a subtree if high accuracy is desired.

These findings are further emphasized by the results in Figure 11 considering Topology 1 with a randomly generated set of load impedances. As we have seen in Figure 6, ranging accuracy is often lower than for fixed load impedances due to larger signal attenuation by low impedance values. Due to this, the distance errors in the recovered trees in Figure 11 are somewhat larger than for the trees in Figure 10. This is particularly true for the full topology in Figure 11(b), with a maximal deviation of 9 m for links connecting nodes 9 and 10. If node 10 is excluded from the tomography, the maximal deviation for the link to node 9 is only 1 m, as can be seen in Figure 11(a).

An example for a reconstructed topology for the Topology 2

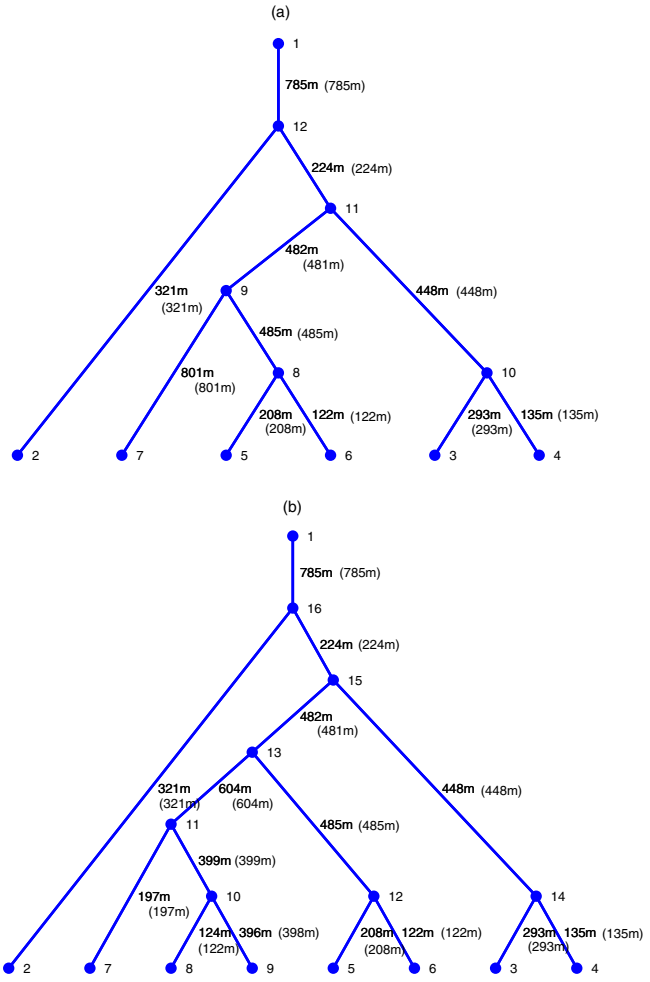

Fig. 12. Example of a reconstructed topology, including distances shown at edges, using the RNJA for Topology 2. MB ranging measurements are used. The numbers in parentheses are the actual distances according to Figure 5. (a): Using node-to-node measurements from seven nodes. Nodes 8 to 12 are created by the RNJA. (b): Using node-to-node measurements from nine nodes. Nodes 10 to 16 are created by the RNJA.

network from Figure 5 is shown in Figure 12. The subfigures (a) and (b) correspond to tomography using node-to-node measurements from seven and nine nodes, respectively. For convenience, we have included the actual distances next to the estimated distances in the edge labels. We observe that also the topology with more branch levels is recovered accurately with distance errors of at most 1 m (Figure 12(a)) and 2 m (Figure 12(b)), respectively. The latter occurs for nodes 8 and 9, likely due their long distances to other nodes and thus less accurate ranging. Comparing the reconstructed trees in Figures 12(a) and (b), we note that the former is a subtree of the latter, and that degree-two nodes (i.e., two edges are connected to a node) cannot be identified.

Finally, Table III summarizes the topology-recovery performance of the proposed method using ED and MB ranging. In particular, the number of instances out of 1000 ranging experiments for which the reconstruction of the correct tree topology can be *guaranteed* are shown. According to [45, Proposition 4], the RNJA returns the correct tree topology if the maximal ranging error is less than half of the minimal link distance, which is 15 m for Topology 1 and 61 m for

TABLE III
NUMBER OF INSTANCES FROM 1000 EXPERIMENTS FOR WHICH CORRECT TOPOLOGY RECONSTRUCTION IS *guaranteed*. RESULTS ARE SHOWN AS A FUNCTION OF NUMBER NODES N. FOR TOPOLOGY 1: NODES $\text{S}\cup\{i : 1 \leq i < N\}$. FOR TOPOLOGY 2: NODES $\{i : 1 \leq i \leq N\}$.

Topology 1, fixed loads									
Ranging mode	Number of nodes								
	3	4	5	6	7	8	9	10	11
ED ($\lambda = 0.1$)	1000	1000	1000	1000	1000	1000	1000	1000	772
MB	1000	1000	1000	1000	1000	1000	1000	1000	1000

Topology 1, varying loads									
Ranging mode	Number of nodes								
	3	4	5	6	7	8	9	10	11
ED ($\lambda = 0.1$)	1000	1000	1000	998	994	985	960	827	22
MB	1000	1000	1000	1000	997	983	945	828	655

Topology 2									
Ranging mode	Number of nodes								
	3	4	5	6	7	8	9	-	-
ED ($\lambda = 0.8$)	1000	1000	1000	1000	1000	1000	936	-	-
MB	1000	1000	1000	1000	998	849	459	-	-

Topology 2. However, this is a sufficient but not a necessary condition, and we have obtained correct tree topologies with the RNJA also for larger ranging errors. The results in Table III confirm the effectiveness of the proposed grid tomography and the detrimental effect of signal attenuation due to low load impedances and large distances. The latter can be mitigated by multiple ranging measurements to improve ranging accuracy (for both MB and ED ranging) and adaptively adjusting the decision threshold λ for ED ranging. Furthermore, smaller partial grid sections can first be reconstructed accurately, and, in a second step, they can be combined into the tree model of the total grid, cf. [48].

VI. CONCLUSIONS

In this paper, we have considered the ability of PLC to retrieve information about the underlying power grid. This is a unique ability of PLC, the only "through-the-grid" communication technology, that has recently received growing attention in the context of smart grid. We have focused on the problem of grid-topology inference using PLC transmission between nodes deployed at the edges of the grid. We have proposed a power grid tomography method that consists of two phases: PLC-based ranging and tree-reconstruction based on distance measurements. To our knowledge, this is the first time that network tomography has been applied to the power grid. Our numerical results have demonstrated the good accuracy of PLC-based ranging, for which we have also proposed a new parametric method. Furthermore, the developed power-grid tomography has shown to be effective. A verification of our simulation results in field trials is still outstanding though. While our original motivation for this work is the use of the proposed power-grid tomography for optimizing PLC networking for smart grids, a broader realm of applications lies in its use for grid monitoring and online diagnostics.

REFERENCES

[1] H. C. Ferreira, H. M. Grov, O. Hooijen, and A. J. Han Vinck, *Power Line Communication*. John Wiley & Sons, 2001. Available: http://dx.doi.org/10.1002/047134608X.W2004

[2] M. Schwartz, "Carrier-wave telephony over power lines: early history," *IEEE Commun. Mag.*, vol. 47, no. 1, pp. 14–18, Jan. 2009.

[3] H. Ferreira, L. Lampe, J. Newbury, and T. Swart (Eds.), *Power Line Communications: Theory and Applications for Narrowband and Broadband Communications over Power Lines*. John Wiley & Sons, 2010.

[4] K. Dostert, M. Zimmermann, T. Waldeck, and M. Arzberger, "Fundamental properties of the low-voltage power distribution grid used as a data channel," *European Trans. Telecommun.*, vol. 11, no. 3, pp. 297–306, May-June 2000.

[5] S. Galli, A. Scaglione, and Z. Wang, "For the grid and through the grid: the role of power line communications in the smart grid," *Proc. IEEE*, vol. 99, no. 6, pp. 998–2017, 2011.

[6] H. Latchman and L. Younge (Guest Editors), "Power line local area networking," *IEEE Commun. Mag.*, vol. 41, no. 4, pp. 32–33, 2003.

[7] S. Galli, A. Scaglione, and K. Dostert (Guest Editors), "Broadband is power: Internet access through the power line network," *IEEE Commun. Mag.*, vol. 41, no. 5, pp. 82–83, 2003.

[8] IEEE Std 1901™-2010, "IEEE Standard for Broadband over Power Line Networks: Medium Access Control and Physical Layer Specifications," Dec. 2010.

[9] S. Bavarian and L. Lampe, "Physical Communications and Access Techniques for Smart Grid," in *Smart Grid Communications and Networking*, E. Hossain, Z. Han, and H. Poor, Eds. Cambridge University Press, 2012.

[10] L. Lampe, A. Tonello, and D. Shaver, "Power line communications for automation networks and smart grid [guest editorial]," *IEEE Commun. Mag.*, vol. 49, no. 12, pp. 26–27, Dec. 2011.

[11] P. Wouters, P. van der Wielen, J. Veen, P. Wagenaars, and E. Fred Steennis, "Effect of cable load impedance on coupling schemes for MV power line communication," *IEEE Trans. Power Delivery*, vol. 20, no. 2, p. 638-645, Apr. 2005.

[12] IEEE Std C37.114™-2004, "IEEE Guide for Determining Fault Location on AC Transmission and Distribution Lines," Jun. 2005.

[13] V. Taylor and M. Faulkner, "Line monitoring and fault location using spread spectrum on power line carrier," *IEE Proc.—Generation, Transmission and Distribution*, vol. 143, no. 5, pp. 427–434, Sep. 1996.

[14] A. N. Milioudis, G. T. Andreou, and D. P. Labridis, "Enhanced protection scheme for smart grids using power line communications techniques—part II: location of high impedance fault position," *IEEE Trans. Smart Grid*, vol. 3, no. 4, pp. 1631–1640, 2012.

[15] R. Rao, S. Akella, and G. Guley, "Power line carrier (PLC) signal analysis of smart meters for outlier detection," in *Proc. 2011 IEEE International Conference on Smart Grid Communications*, pp. 291–296.

[16] M. Smail, L. Pichon, M. Olivas, F. Auzanneau, and M. Lambert, "Detection of defects in wiring networks using time domain reflectometry," *IEEE Trans. Magn.*, vol. 46, no. 8, pp. 2998–3001, Aug. 2010.

[17] M. Ahmed and L. Lampe, "Power line network topology inference using frequency domain reflectometry," in *2012 IEEE International Conference on Communications*.

[18] T. Erseghe, F. Lorenzon, S. Tomasin, A. Costabeber, and P. Tenti, "Distance measurement over PLC for dynamic grid mapping of smart micro grids," in *Proc. 2011 IEEE Smart Grid Communications*, pp. 487–492.

[19] A. Costabeber, P. Tenti, T. Erseghe, S. Tomasin, and P. Mattavelli, "Distributed control of smart microgrids by dynamic grid mapping," in *Proc. 2011 Conference of IEEE Industrial Electronics Society*, pp. 1323–1328.

[20] T. Erseghe, S. Tomasin, and A. Vigato, "Topology estimation for smart micro grids via powerline communications," *IEEE Trans. Signal Process.*, vol. 61, no. 13, pp. 3368–3377, Jul. 2013.

[21] F. Cañete, J. Cortés, L. Díez, and J. Entrambasaguas, "Modeling and evaluation of the indoor power line transmission medium," *IEEE Commun. Mag.*, vol. 41, no. 4, pp. 41–47, Apr. 2003.

[22] A. Tonello and F. Versolatto, "Bottom-up statistical PLC channel modeling—part I: random topology model and efficient transfer function computation," *IEEE Trans. Power Delivery*, vol. 26, no. 2, pp. 891–898, Apr. 2011.

[23] P. Stoica and R. L. Moses, *Introduction to Spectral Analysis*. Prentice-Hall, 1997.

[24] R. Castro, M. Coates, G. Liang, R. Nowak, and B. Yu, "Network tomography: recent developments," *Statistical Science*, vol. 19, no. 3, pp. 499–517, 2004.

[25] G. Bumiller, L. Lampe, and H. Hrasnica, "Power line communication networks for large-scale control and automation systems," *IEEE Commun. Mag.*, vol. 48, no. 4, pp. 106–113, Apr. 2010.

[26] L. Lampe and A. Vinck, "On cooperative coding for narrowband PLC networks," *International J. Electron. and Commun.*, vol. 65, no. 8, pp. 681–687, Aug. 2011.

[27] M. Biagi and L. Lampe, "Location assisted routing techniques for power line communication in smart grids," in *2010 IEEE International Conference on Smart Grid Communications.*

[28] M. Mauve, A. Widmer, and H. Hartenstein, "A survey on position-based routing in mobile ad hoc networks," *IEEE Network*, vol. 15, no. 6, pp. 30–39, Nov./Dec. 2001.

[29] M. Kezunovic, "Smart fault location for smart grids," *IEEE Trans. Smart Grid*, vol. 2, no. 1, pp. 11–22, Mar. 2011.

[30] S. Goldfisher and S. Tanabe, "IEEE 1901 access system: an overview of its uniqueness and motivation," *IEEE Commmun. Mag.*, vol. 48, no. 10, pp. 150–157, Oct. 2010.

[31] L. Dho and R. Lehnert, "Dynamic resource allocation protocol for large PLC networks," in *Proc. 2012 IEEE Intl. Symp. Power Line Commun.*, pp. 41–46.

[32] G. Prasanna, A. Lakshmi, S. Sumanth, V. Simba, J. Bapat, and G. Koomullil, "Data communication over the smart grid," in *Proc. 2009 IEEE Intl. Symp. Power Line Commun.*, pp. 273–278.

[33] D. Dardari, A. Conti, U. Ferner, A. Giorgetti, and M. Win, "Ranging with ultrawide bandwidth signals in multipath environments," *Proc. IEEE*, vol. 97, no. 2, pp. 404–426, Feb. 2009.

[34] A. A. D'Amico, U. Mengali, and L. Taponecco, "Energy-based TOA estimation," *IEEE Trans. Wireless Commun.*, vol. 7, pp. 838–847, Mar. 2008.

[35] M. Zimmermann and K. Dostert, "A multipath model for the powerline channel," *IEEE Trans. Commun.*, vol. 50, no. 4, pp. 553–559, Apr. 2002.

[36] Y. Bresler and A. Macovski, "Exact maximum likelihood parameter estimation of superimposed exponential signals in noise," *IEEE Trans. Acoust., Speech, Signal Process.*, vol. 34, no. 5, pp. 1081–1089, 1986.

[37] R. Kumaresan and D. Tufts, "Estimating the parameters of exponentially damped sinusoids and pole-zero modeling in noise," *IEEE Trans. Acoust., Speech, Signal Process.*, vol. 30, no. 6, pp. 833–840, Dec. 1982.

[38] M. Rahman and K.-B. Yu, "Total least squares approach for frequency estimation using linear prediction," *IEEE Trans. Acoust., Speech, Signal Process.*, vol. 35, no. 10, pp. 1440–1454, Oct. 1987.

[39] Y. Hua and T. Sarkar, "Matrix pencil method for estimating parameters of exponentially damped/undamped sinusoids in noise," *IEEE Trans. Acoust., Speech, Signal Processing*, vol. 38, no. 5, pp. 814–824, 1990.

[40] I. Maravic and M. Vetterli, "Sampling and reconstruction of signals with finite rate of innovation in the presence of noise," *IEEE Trans. Signal Process.*, vol. 53, no. 8, pp. 2788 – 2805, Aug. 2005.

[41] M. Wax and T. Kailath, "Detection of signals by information theoretic criteria," *IEEE Trans. Acoust., Speech, Signal Process.*, vol. 33, no. 2, pp. 387 – 392, apr 1985.

[42] V. Reddy and L. Biradar, "SVD-based information theoretic criteria for detection of the number of damped/undamped sinusoids and their performance analysis," *IEEE Trans. Signal Process.*, vol. 41, no. 9, pp. 2872–2881, sep 1993.

[43] F. Cañete, J. Cortés, L. Díez, and J. Entrambasaguas, "Analysis of the cyclic short-term variation of indoor power line channels," *IEEE J. Sel. Areas Commun.*, vol. 24, no. 7, pp. 1327–1338, Jul. 2006.

[44] J. Cortés, L. Díez, F. Cañete, J. Sánches-Martínez, and J. Entrambasaguas, "Performance analysis of OFDM modulation on indoor broadband PLC channels," *EURASIP J. Advances in Signal Process.*, vol. 2011, 2011.

[45] J. Ni and S. Tatikonda, "Network tomography based on additive metrics," *IEEE Trans. Inf. Theory*, vol. 57, no. 12, pp. 7798–7809, Dec. 2011.

[46] N. Saitou and M. Nei, "The neighbor joining method: a new method for reconstructing phylogenetic trees," *Molecular Biology and Evolution*, vol. 4, no. 4, pp. 406–425, 1987.

[47] J. Ni, H. Xie, S. Tatikonda, and Y. Yang, "Efficient and dynamic routing topology inference from end-to-end measurements," *IEEE/ACM Trans. Networking*, vol. 18, no. 1, pp. 123–135, 2010.

[48] L. Lampe and M. Ahmed, "Power grid topology inference using power line communications," in *2013 IEEE International Conference on Smart Grid Communications.*

[49] Nexans, "Power cables 1-30 kV," Edition 2002. Available: http://www.nexans.de/eservice/Germany-de_DE/documentDownload_312/

[50] A. Lotito, R. Fiorelli, D. Arrigo, and R. Cappelletti, "A complete narrowband power line communication node for AMR," in *Proc. 2007 IEEE Intl. Symp. Power Line Commun.*, pp. 161–166.

[51] T. Banwell and S. Galli, "On the symmetry of the power line channel," in *Proc. 2001 Intl. Symp. Power Line Commun.*, pp. 325–330.

Mohamed Osama Ahmed received the BSc degree in Electronics and Communications Engineering from Cairo University, Egypt in 2006, and the MSc degree in Engineering Physics from Cairo University in 2010. In 2013, he received the MASc degree in Electrical and Computer Engineering from the University of British Columbia, Canada. Afterward, he received the Four Year Doctoral Fellowship (4YF) to pursue the PhD degree in the Department of Computer Science at the University of British Columbia. His research interests lie broadly in the areas of machine learning, speech recognition, and signal processing.

Lutz Lampe (M'02, SM'08) received his Diplom (Univ.) and Ph.D. degrees in electrical engineering from the University of Erlangen, Germany, in 1998 and 2002, respectively. Since 2003 he has been with the Department of Electrical and Computer Engineering at the University of British Columbia, where he is a full profssor. His research interests are broadly in theory and application of wireless, optical wireless and power line communications. He is (co-)recipient of a number of Best Paper Awards, including award at the 2006 IEEE International Conference on Ultra-Wideband (ICUWB), 2010 IEEE International Communications Conference (ICC) and 2011 IEEE International Conference on Power Line Communications (ISPC). He was awarded the Friedrich Wilhelm Bessel Research Award by the Alexander von Humboldt Foundation in 2009. He is an Associate Editor for the IEEE WIRELESS COMMUNICATIONS LETTERS and the IEEE COMMUNICATIONS SURVEYS AND TUTORIALS, and has served as Associate and Guest Editor for several IEEE transactions and journals. He was the General Chair of ISPLC 05 and IEEE ICUWB 09 and General Co-Chair of 2013 IEEE International Conference on Smart Grid Communications (SmartGridComm). He is the Chair of the IEEE Communications Society Technical Committee on Power Line Communication.